First-principles density-functional study of metal-carbonitride interface adhesion: Co/TiC(001) and Co/TiN(001)

S. V. Dudiy* and B. I. Lundqvist
Department of Applied Physics, Chalmers University of Technology and Göteborg University, SE-412 96 Göteborg, Sweden
(Received 17 January 2001; published 28 June 2001)

The energetics and the electronic structure of fcc Co(001)/TiC(001) and Co(001)/TiN(001) interfaces, which are of much practical importance in the sintering of hardmetals, are investigated by means of first-principles density-functional calculations, using the plane-wave pseudopotential method. The effects of the large Co/Ti(C,N) lattice mismatch are incorporated within an approach based on a comparative analysis of a representative set of high-symmetry model interface structures. It is shown that the dominating mechanism of the Co/Ti(C,N) interface adhesion is strong covalent σ bonding between Co-3d and C(N)-2p orbitals. An extensive analysis of the electronic structure elucidates the interface-induced features of the Co-C(N) bonding and antibonding electronic states that are responsible for the enhanced strength of the interface Co-C(N) compared to bonds in bulk carbonitrides, the effect describable as metal-modified covalent bond. A detailed comparison of the energetics and relaxation effects at the Co/TiC and Co/TiN interfaces shows a weaker bonding and less pronounced relaxation effects in the Co/TiN case, which can be connected to the experimentally observed difference in the stability of those interfaces. The weaker Co/TiN adhesion is explained in terms of the relative position of the energy region of the N-2p states with respect to the Co-3d states. The calculated adhesion strength is consistent with the available data from wetting experiments with liquid Co on a TiC surface.

DOI: 10.1103/PhysRevB.64.045403 PACS number(s): 68.35.−p, 71.15.Nc, 73.20.−r, 81.05.Je

I. INTRODUCTION

A unique combination of properties found in transition-metal carbides and nitrides makes them particularly interesting from both technological and scientific points of view. Here ultrahardness and high melting points, typical of covalent compounds, coexist with metallic conductivity. At the same time, many of these carbides and nitrides have a NaCl structure, a typical feature of ionic crystals. The brittleness of the carbonitrides is the reason why, in technological applications, in particular in the cutting-tool industry, they are used in the form of cemented carbides and cermets,[1,2] materials produced by sintering carbonitride powder with a powder of a tough binder metal. Both the sintering process and the performance of the final product are to a large extent controlled by the interfaces between the carbonitride grains and the binding metal phase. In this context, an understanding of metal-carbonitride bonding at the atomic level, a very valid goal for fundamental science, could stimulate ideas for further technological developments.

For a long time, the dominating type of hard metal has been WC-Co, often with the addition of TiC and other cubic carbides. An important reason for this is its very good wetting (wetting angle equals zero), making it possible to sinter to a pore-free material, even at atmospheric pressure, and providing very good mechanical properties. In attempts to eliminate WC for improved hardness and wear resistance, wetting is a key parameter. Nitrogen is now also being introduced into hardmetal systems. Most materials (so-called ''cermets'') in this extensive development are based on Ti(C,N) and a metal binder phase, Ni+Co, or preferably cobalt alone.

It is a rather long-winded process to make and study different test materials and to try to understand the reasons for variations in the properties (of which wetting is only one component). Therefore, it would be of great value to be able to predict the wetting behavior of different systems. Thus Co/Ti(C,N) is the given first system to study.

In materials theory a number of approaches to the energetics and electronic structure of metal-ceramic interfaces have been developed during the last two decades.[3,4] They include simplified scattered-wave,[5] atomic-orbital,[6] tight-binding,[7–10] and image-interaction[11–13] models, as well as first-principles density-functional-theory calculations.[14–23] However, so far the most extensively studied metal-ceramic interfaces are those where the described ceramic is a wide-band-gap ionic oxide, like MgO (Refs. 13–18) or alumina,[19–21] while the situations of transition-metal carbides and nitrides are still quite unexplored.

Existing attempts to elucidate the nature of the metal-carbide adhesion were mainly confined to extracting information on the bonding mechanism from the analysis of correlations between the wetting behavior and the electronic properties of various carbides (reviewed in Refs. 1 and 24). The linear dependence of the work of adhesion on the energy shift of the C 1s electrons, shown in Ref. 25, is interpreted in terms of an ionic bonding, and allows one to establish a relation between wetting and carbide, stability: the more stable the carbide, the smaller the wettability. The same relation was found in Ref. 26, assuming covalent bonding. In Ref. 27 it was shown that the work of adhesion depends linearly on the carbide free-electron concentration, which supports a metallic bonding picture. More recently,[24] trends in the wetting behavior of liquid copper on metal carbides were claimed to fit the predictions of the dielectric continuum model of Barrera and Duke well,[28] which would mean that the main contribution to the bonding could be attributed to dispersion forces; however, this was questioned in Ref. 29. In spite of the attempts to understand the metal-

carbide interactions on the basis of trends, the atomistic nature of bonding remains an open question. More decisive conclusions on the role of different bonding mechanisms require detailed studies of the interface electronic structure and energetics.

Extending and continuing our recent paper,[30] the present paper explores the relation between the energetics and the details of the atomic and electronic structures of the Co/TiC(001) and Co/TiN(001) interfaces, by means of first-principles electron-structure calculations based on density-functional theory[31–33] at the generalized gradient approximation (GGA) level. As measures of the interface energetics, the interface energy and the ideal work of separation are used. The atomic structure is determined by a minimization of the total-energy density functional under the constraints given in each case studied. The electron structure is described in terms of the valence electron density, the electronic density of states, and the spatial distribution of the electron-density contributions from separate Kohn-Sham bands. It has been analyzed in the context of the theory of bonding in bulk carbides and nitrides.[34,35] We show that the dominating mechanism of the Co/Ti(C,N) interface adhesion is strong covalent σ bonding between the $3d$ orbitals of cobalt and the $2p$ orbitals of carbon or nitrogen. Moreover, our previously reported result,[30] that the Co/TiC interface Co-C bonds are significantly stronger than the bonds in bulk CoC, or even in bulk TiC, is now also found for Co/TiN, and is investigated in a greater detail. In addition, a detailed comparison of the adhesion in Co/TiC and Co/TiN is made.

The paper is organized as follows. Section II specifies the model systems to be studied, and discusses our methodology. The computational method used and the details of the calculations are accounted for in Sec. III, where the results of extensive test calculations of bulk properties of Ti, Co, TiC, TiN, CoC, and CoN, along with surface properties of TiC and TiN, are also provided. The results of our interface calculations are presented and discussed in Sec. IV. Section V summarizes our conclusions.

II. FORMULATION OF PROBLEM AND METHODOLOGY

Very little is known about the energetics and structure of cermet interfaces. The primary goal of the present study is therefore to be explorative. For practical reasons, an unlimited computational search for the structure is out of question. We have to start with restricted searches on model systems that are simple enough to be possible to perform on the computer and yet complex enough to reveal the key physical features. Unfortunately, structural clues from experiments are very few. In the following we give some arguments for the model systems that we have chosen to study.

So far no simple epitaxial interface between Co and TiC or TiN has been obtained in experiment. A key reason for this is probably the large lattice mismatch between bulk Co and TiC or TiN, about 25% (Table I and Fig. 1). The only available experimental prototypes of the considered model systems are heterophase boundaries in the Co-Ti(C,N) cermets, and interfaces between liquid Co and TiC in wetting experiments.[36]

We choose to focus on the interfaces formed by the paramagnetic fcc Co phase and the (001) surfaces of TiC and TiN. Experimentally, up to 418 °C the stable state of pure Co is ferromagnetic hcp.[37] However, in the binder phase of the sintered carbides residual stresses and the presence of carbon and tungsten can stabilize the high-temperature fcc structure of Co even at room temperature.[37] For the titanium carbide in its NaCl structure, the (001) plane is a well-defined cleavage plane.[38] This makes the TiC(001) surface one of the most common faces of the TiC powder grains.[39] For nearly stoichiometric TiC, the shape of the powder grains is retained during the sintering.[1] These observations suggest that the fcc Co/TiC(001) interfaces represent very realistic situations. Some analogous features are also expected in the case of TiN, because of the similarity of the TiC and TiN structural and electronic properties.

The complexity of the atomic structure of realistic Co/Ti(C,N) interfaces makes it impossible to do a brute-force first-principles modeling in the same sense as for well-matched epitaxial interfaces. A common way around this difficulty is to use simplified models for interatomic interactions. However, the lack of understanding about the nature of metal-carbonitride interface interactions leaves practically no basis for any reliable interaction models. A more adequate strategy is to keep the accurate treatment of the electronic structure given by the first-principles methods, at the expense of having a more qualitative description of the interface atomic structure. Such a first-principles analysis can provide many valuable insights, which are typically difficult to extract from experiment.

Following the above strategy, we attempt to obtain a basic understanding of complex-structured interfaces by considering a series of high-symmetry model systems. On the one hand, if we assume that the behavior of each atom is dominated by its local environment, then such model systems can cover a representative set of different local atomic configurations. This can be used to identify different possible types of local behaviors. On the other hand, comparing the properties of different model systems, we can extract features that are retained from one structure to another and, hence, can survive at a generic complex-structured interface.

As model systems we choose different high-symmetry rotation and translation states of the interface that can be formed between the (001) surface of Ti(C,N) and the (001) surface of fcc Co (see Figs. 1 and 2). On the scale of the energies required to distort the very stable rocksalt structures of TiC and TiN, the energy difference between the different Co phases is small. In view of this fact, in constructing commensurate interface structures the lattice constant of TiC or TiN is kept as the unstrained-bulk one, while a change of the in-plane lattice constant of the Co layers is allowed. We also take into account that the Co in-plane distortion induces a change of the Co interlayer separation (the Poisson effect).

High-symmetry rotation states of the Co(001)/Ti(C,N)(001) interface, all periodic with reasonably small unit cells, are generated by matching the two-dimensional square unit cells of the translation vector lattices for the Ti(C,N)(001) and Co(001) surface layers by adjusting the Co in-plane lattice constant (Fig. 1). The rotation states obtained

TABLE I. Equilibrium lattice constants a_0, bulk moduli B, and cohesive energies E_{coh}, of Ti, TiC, TiN, Co, CoC, and CoN: values from present plane-wave pseudopotential (PWPP) calculations and compared with the results of other calculations and experimental (Expt) data.

Crystal	Method	Source	a_0 (Å)	B (Mbar)	E_{coh} (eV)
Ti(hcp)	GGA-PWPP	This work	2.92	1.12	5.1
	GGA-FP-LMTO	Ref. 43	2.917	1.08	-
	Exp	Ref. 53	2.95	1.05	4.85
Ti(fcc)	GGA-PWPP	This work	4.11	1.06	5.1
	GGA-LMTO-ASA	Ref. 59	4.22	1.08	4.5
TiC	GGA-PWPP	This work	4.33	2.52	7.3
	GGA-FP-LMTO	Ref. 44	4.315	2.2	-
	Expt	Ref. 54	4.317	2.4	-
	Expt	Quoted in Ref. 34	4.33	-	7.16
TiN	GGA-PWPP	This work	4.25	2.78	6.8
	GGA-FP-LMTO	Ref. 44	4.230	2.7	-
	Expt	Ref. 54	4.240	3.2	-
	Expt	Quoted in Ref. 34	4.24	-	6.69
Co(hcp) FM	GGA-PWPP	This work	2.49	2.16	5.3
	GGA-PWPP	Ref. 58	2.51	2.05	-
	GGA-LMTO-ASA	Quoted in Ref. 58	2.52	2.24	-
	Expt	Ref. 53	2.51	1.91	4.39
Co(fcc) FM	GGA-PWPP	This work	3.52	2.11	5.3
	GGA-PWPP	Ref. 58	3.52	2.05	-
	GGA-LMTO-ASA	Quoted in Ref. 58	3.53	2.37	-
Co(fcc) NM	GGA-PWPP	This work	3.45	2.53	5.2
CoC	GGA-PWPP	This work	4.01	3.08	5.8
	Expt	Quoted in Ref. 34	4.05	-	5.7
	LDA-LMTO-ASA	Ref. 34	-	-	7.8
CoN	GGA-PWPP	This work	4.00	3.02	4.7
	Expt	Quoted in Ref. 34	4.10	-	4.5
	LDA-LMTO-ASA	Ref. 34	-	-	6.5

in this way are denoted nCo/mTi(C,N), where the integers n and m indicate that in the unit cell of the resulting interface structure there are n surface atoms of Co per m surface atoms of Ti or C(N). An elementary geometrical analysis shows that for a square unit cell of a square lattice the allowed values of n and m are representable as $m,n=l^2+k^2$, where l and k are arbitrary integers. The choice is here restricted to three different rotation states: 1Co/1Ti(C,N), 5Co/4Ti(C,N), and 8Co/5Ti(C,N) (Fig. 2). The 1Co/1Ti(C,N) interfaces provide simple illustrations of the effects that are also present in complex cases. The 8Co/5Ti(C,N) interfaces represent the situation with a moderate, within 5%, elastic strain of the Co layers. The 5Co/4Ti(C,N) rotation state is an intermediate case with respect to both strain and complexity. The rotation states excluded in Fig. 2 and in the calculations either involve too large a Co distortion or require larger interface unit cells without any promise of new qualitative features.

The high-symmetry translation states are distinguished by the presence of a fourfold axial symmetry, i.e., a fourfold symmetry axis of the Ti(C,N) surface coincides with a fourfold axis of the Co surface. A symmetry analysis shows that for each of the three chosen rotation states, nCo/mTi(C,N), there are only two different high-symmetry translation states, here enumerated by nCo/mTi(C,N)-I and nCo/mTi(C,N)-II. The rotation and translation states of all the considered high-symmetry model systems are summarized in Fig. 2, where the position of the Co surface layer with respect to the Ti(C,N) surface is displayed, all within one interface unit cell.

To save computational effort and to simplify analysis, this pilot study considers only the paramagnetic state of Co. For Co/TiC, the role of the Co ferromagnetism was analyzed in Ref. 40, where it was shown that the magnetism is not crucial for our present conclusions. The magnetic corrections to the interface energetics are reasonably well reproducible within a rigid-band approach, as for free Co surfaces,[41] taking as an input the density of the electronic states from the paramagnetic case.

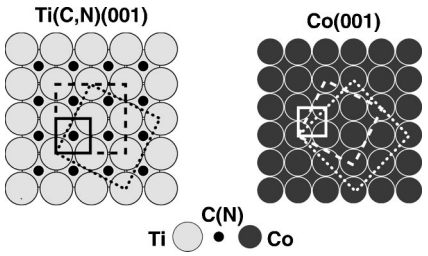

FIG. 1. Different possible unit cells (the square frames) for the (001) surfaces of Ti(C,N) and fcc Co. By adjusting the in-plane lattice constant of the Co phase, one can make one of the unit cells of Co(001) the same size as some unit cell of Ti(C,N)(001). In this way periodic Co(001)/Ti(C,N)(001) interfaces can be obtained. The unit-cell frames shown by continuous, dashed, and dotted lines are used to construct 1Co/1Ti(C,N), 5Co/4Ti(C,N), and 8Co/5Ti(C,N) interfaces, respectively.

III. COMPUTATIONAL METHOD

The general framework of the used computational method is the density functional-theory,[31–33] with the exchange-correlation energy treated in the generalized gradient approximation. We use the PERDEW-WANG91 version of the GGA (GGA-PW91),[42] which has been shown to give a reliable and accurate description of the bulk ground-state properties of both transition metals[43] and titanium carbides and nitrides.[44] The self-consistent total-energy calculations are performed with the plane-wave pseudopotential method[45–47] implemented in the dacapo code.[48] All the involved elements (Co,Ti,C,N) are described by Vanderbilt ultrasoft pseudopotentials,[49] which substantially decreases the necessary number of plane waves in the basis set. For the Ti and Co pseudopotentials the nonlinear core correction[50] is used. The plane-wave cutoff is taken to be 26 Ry (354 eV), which provides a good total-energy convergence of about 0.01 eV/atom. The Brillouin zone is sampled according to the Monkhorst-Pack method.[51] To improve the *k*-point convergence, the Fermi discontinuity is smoothed using the Gillan scheme,[52] with the effective electronic temperature 0.15 eV. The number of *k* points is chosen to provide a similar level of the total-energy convergence as with respect to the cutoff energy. The specific size of the *k*-point mesh used will be given below for each system studied.

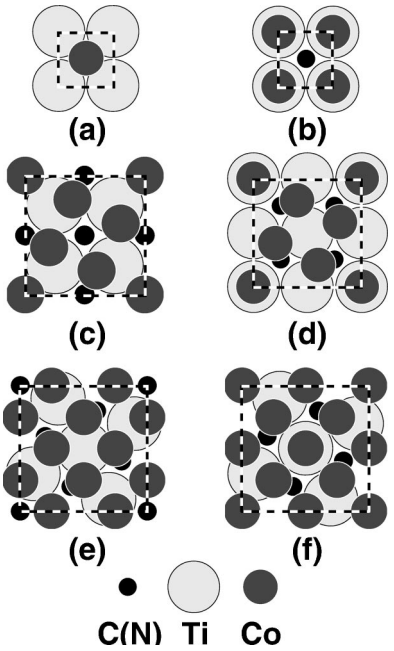

FIG. 2. Relative positions of the first Co layer with respect to the Ti(C,N) surface layer for the considered interface geometries. (a) 1Co/1Ti(C,N)-I: Co atom over C(N) atom. (b) 1Co/1Ti(C,N)-II: Co atom over Ti atom. (c) 5Co/4Ti(C,N)-I. (d) 5Co/4Ti(C,N)-II. (e) 8Co/5Ti(C,N)-I. (f) 8Co/5Ti(C,N)-II.

To assess the reliability of our computational method, in particular of the pseudopotentials used, extensive calculations for the bulk properties of Ti, TiC, TiN, Co, CoC, and CoN have been performed. The calculated values of the lattice constant, bulk modulus, and cohesive energy for each material are presented in Table I, together with available data from other calculations and experiment. The lattice constants, the bulk moduli, and the bulk total energies are obtained by fitting the Murnaghan equation of state[55] to the total energies calculated at different volumes. The cohesive energies are evaluated as the difference between the bulk and atomic total energies. For spin-polarized atomic calculations an 8-Å-sided cubic supercell is used, and the Brillouin zone is sampled with the Γ point only.

Here we compare the results of our GGA-PW91 ultrasoft pseudopotential (USPSP) calculations with available results of the GGA or local-density-approximation (LDA) full-potential (FP) calculations. Our calculated values for the c/a ratio, 1.58, and the equilibrium volume of hcp Ti agree within 0.5% and 0.1%, respectively, with the results of the GGA-PW91 full-potential (FP) linear-muffin-tin-orbital (LMTO) calculations.[43] The bulk modulus is only overestimated by 4%. The structural energy difference obtained between hcp and fcc Ti, 0.05 eV/atom, is close to the result (0.06 eV/atom) of LDA FP-LMTO calculations.[56] The pseudopotential used for Co (Ref. 57) is similar to the one in Ref. 58, and provides similar agreement with the FP results. We obtain that the ferromagnetic (FM) hcp phase of Co is 0.02 eV/atom lower in energy than ferromagnetic fcc, and the c/a ratio for hcp Co is 1.62. The calculated magnetic moments are 1.55μ and 1.60μ per atom for the hcp and fcc Co phases, respectively, where μ is the Bohr magneton.

For TiC and TiN (Table I) the calculated equilibrium volumes are within less than 1% of the GGA FP-LMTO values,[44] while the bulk modulus values are overestimates, 15% for TiC and 3% for TiN. It is known[34] that the LDA leads to noticeable overestimation, by more than 25%, of the experimental cohesive energies of transition-metal carbides and nitrides. Our GGA-PW91 results for the TiC and TiN cohesive energies agree within 5% with the experimental values listed in Ref. 34.

As the Co-C and Co-N bonds are expected to play important roles in the Co/Ti(C,N) interface bonding, we also consider bulk CoC and CoN in the NaCl structure (Table I). Although experimentally unstable, these compounds were studied previously[34] in the context of the systematics of the bonding properties. Our calculated cohesive energies of CoC

TABLE II. Calculated values of the surface energy (in J/m^2) for unrelaxed (Unrel) and relaxed (Rel) TiC(001) and TiN(001) surfaces.

TiC(001)		TiN(001)	
Unrel	Rel	Unrel	Rel
1.84	1.71	1.64	1.36

and CoN are in good agreement with the values[34] estimated from the experimental data.

For future reference we also calculate the TiC(001) and TiN(001) surface properties. The calculations are performed in a slab geometry with a fixed-height, 14-layer, supercell. An $8\times8\times2$ Monkhorst-Pack *k*-point grid is used. The thicknesses of the TiC and TiN slabs are varied from three to ten layers, and the surface energies are extracted using the method of the linear fit to the slab energies, as described in Ref. 60. Three-layer slabs are enough to provide a convergence of the surface-energy values with respect to the number of layers to a value of about 0.03 J/m^2. The relaxation energies are calculated for seven-layer slabs, allowing relaxation of one surface layer on each side of the slab. For the relaxed structures the ionic forces are less than 0.05 eV/Å.

The calculated surface energies for TiC(001) and TiN(001) are presented in Table II. The obtained relaxation of the TiC(001) surface is Ti0.07 Å inward and C0.04 Å outward. This gives a surface rippling, i.e., a difference in C and Ti displacements, of $r=0.12$ Å. Compared to the predictions of the LDA FP-LMTO calculation,[61] where Ti moves 0.04 Å inward and C0.02 Å outward, the relaxation is of the same type but with a larger magnitude. At the same time our result is still consistent with the experimental work,[63] which shows $r\leqslant0.1$. It is also in reasonable agreement with recent highly accurate measurements,[62] where the TiC(001) relaxation is Ti0.036 Å inward and C0.040 Å outward. TiN(001) has the same direction of relaxation, but the magnitude is about twice as large, Ti0.12 Å inward and N0.06 Å outward.

In summary, we find that the computational method we used provides an adequate description of the structural, elastic, and cohesive properties of all the considered materials.

IV. RESULTS AND DISCUSSION

The Co(001)/Ti(C,N)(001) interface is modeled in a supercell geometry, following the methodology discussed in Sec. II. For TiC and TiN slabs, the optimized lattice constants used are 4.331 and 4.245 Å, respectively. The structure and energetics of the strained fcc Co phases used in our calculations are summarized in Table III. For a given interface rotational state, the in-plane lattice constant of Co is adjusted to have commensurate structures with the Ti(C,N) slabs. Then for each choice of the in-plane lattice constant the out-of-plane lattice constant of Co is optimized in an additional set of bulk calculations. This is done in order to minimize the Co strain energy.

It is worth noting that the considered Co structures can also be viewed as body-centered-tetragonal (bct) structures with different values of the c/a ratio. At $c/a=\sqrt{2}$ we have a fcc structure, while $c/a=1$ gives a bcc structure. The c/a values in Table III show that the Co structures for the 5Co/4Ti(C,N) case are closer to bcc than to fcc. The 1Co/1Ti(C,N) case, $c/a=0.8$, is even farther from fcc, but the strain energy is less than for 5Co/4Ti(C,N). A similar behavior of the strain energy versus the bct c/a ratio has been found for the FM Co.[64,58] The LDA FP (Ref. 64) and USPSP (Ref. 58) calculations show that at fixed volume the strain energy versus the c/a ratio has a minimum at $c/a=\sqrt{2}$ (fcc),

TABLE III. The strained paramagnetic (PM) fcc Co structures matched to the Ti(C,N)(001) surface: bulk and surface calculations. The first column indicates for which interface the given Co phase is to be used. The (001)-plane lattice constant a_{xy}($a_0=3.452$ Å); the interlayer distance d_z($d_0=a_0/2$); the strain energy per layer, E_{str}; the bct c/a ratio; and the (001) surface energy (unrelaxed and relaxed) are given. For comparison, also shown are calculated values of the (001) surface energy for unstrained (Unstr.) PM and ferromagnetic (FM) Co, and the corresponding values from the LDA LMTO-ASA calculations of Ref. 41.

Interface	a_{xy}/a_0	d_z/d_0	E_{str} (J/m^2)	c/a	E_{surf} (J/m^2)	
					Unrel	Rel
1Co/1TiC	1.255	0.691	0.400	0.78	3.04	2.96
5Co/4TiC	1.122	0.847	0.505	1.07	2.73	2.62
8Co/5TiC	0.992	1.008	0.0044	1.44	3.04	2.98
1Co/1TiN	1.230	0.698	0.351	0.80	3.04	2.97
5Co/4TiN	1.100	0.896	0.411	1.15	2.82	2.69
8Co/5TiN	0.972	1.026	0.063	1.49	3.03	2.98
Unstr. Co (PM)	1.000	1.000	0.000	1.41	3.04	2.97
Unstr. Co (FM)	-	-	-	-	2.67	2.63
Unstr. Co (PM) (Ref. 41)	-	-	-	-	3.40	-
Unstr. Co (FM) (Ref. 41)	-	-	-	-	2.78	-

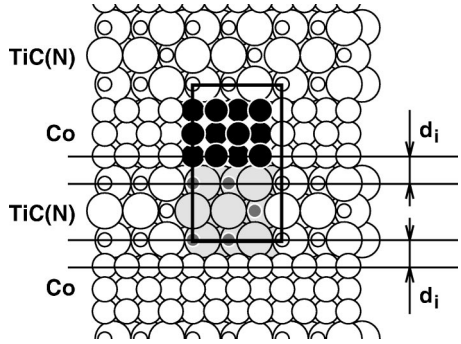

FIG. 3. An example of the interface supercells. A side view of the (3+3)-layer supercell for the unrelaxed 8Co/5Ti(C,N)-I interface is displayed. The atoms within one supercell (shaded circles) and their periodic images (blank circles) are shown. In the Ti(C,N) slabs the larger and smaller circles correspond to Ti and C(N) atoms, respectively. Here d_i is the interface interlayer separation referred to in the text.

a local maximum at $c/a=1$ (bcc), and a shallow local minimum near $c/a=0.9$.

The Co surface energies (Table III) are calculated in the same way as for Ti(C,N)(001) (Table II). In spite of the noticeable distortion of Co, the surface-energy values differ relatively little from those of the unstrained Co. For comparison, we also present our calculated values for the unstrained FM fcc (001) Co surface energy (Table III). The surface-energy values in Table III for unstrained fcc Co(001) are consistent with the LDA LMTO-ASA (atomic sphere approximation) results of Ref. 41.

At the first step of our interface calculations, the Co and Ti(C,N) slabs are taken as ideal truncations of the corresponding bulk structures. The lateral size of the supercell and the relative positions of the slabs are chosen in accordance with the given interface rotation and translation states (Fig. 2). In this step only the distance between the slabs, the interface interlayer separation, is optimized to minimize the total energy of the system. The structures constructed in this way are regarded as unrelaxed interface systems. An example of a supercell for an unrelaxed interface is shown in Fig. 3.

At the next step, all the atoms of the outermost layers of each slab are allowed to relax until the total residual forces on the relaxed atoms are less than 0.1 eV/Å. The positions of the remaining atoms and the supercell size are kept fixed. Monkhorst-Pack k-point grids of sizes $8\times8\times2$, $4\times4\times2$ and $2\times2\times2$ are used for 1Co/1Ti(C,N), 5Co/4Ti(C,N), and 8Co/5Ti(C,N) interfaces, respectively. Convergence tests done for the 8Co/5TiC-I system show that going from a $2\times2\times2k$-point mesh to a $4\times4\times2$ mesh changes the interface energetics by less than 0.05 J/m^2, and increasing the plane-wave cutoff to 40 Ry gives a change in the interface energy of less than 0.01 J/m^2.

For many of the considered model systems (Fig. 2), we need supercells with relatively large lateral sizes. To keep the computational cost at a reasonable level, the major part of the calculations is performed with supercells containing three layers of each material [(3+3)-layer supercells, with up to 54 atoms in the supercell]. To estimate how well converged our results are with respect to the number of Co and Ti(C,N) layers, we choose a few of the most representative interface structures [1Co/1Ti(C,N)-I,II and 8Co/5Ti(C,N)-I] and make the final tests using 5+5 supercells (up to 90 atoms in the supercell). For such tests the optimized interface interlayer separation is taken from the (3+3)-supercell calculations. In the tables referred to below, the values obtained with 5+5 supercells are given in parentheses. The results of the tests show that, for the main conclusions drawn below, the results with the (3+3)-layer supercells are sufficiently converged.

A. Atomic structure and energetics

The strength of the interface bonding can be described by the *ideal work of separation*, W_{sep}, which is the work per unit area of interface required to separate the interface reversibly, thus creating two free surfaces. We calculate W_{sep} as in Ref. 19, i.e., as

$$W_{sep}=(E_{sl1}+E_{sl2}-E_{int})/2A, \tag{1}$$

where E_{int} is the total energy of the supercell with the interface system; E_{sl1} and E_{sl2} are the total energies of the same supercell when one of the slabs is kept and the other one is replaced by vacuum, and A is the interface area within one supercell. The factor 2 in the denominator accounts for the fact that there are two (identical) interfaces per supercell (see Fig. 3). To calculate W_{sep}, for the relaxed interface structures the relaxed values of E_{sl1} and E_{sl2} are used.

Another useful characteristic of the interface energetics is the *interface energy*, i.e., the excess free energy associated with a unit area of interface. The interface energy shows how much weaker the bonding is at the interface than the interlayer bonding in the corresponding bulk materials. This quantity is quite often used in thermodynamical modeling, e.g., in metallurgical research, and it can be calculated as

$$\gamma=(E_{int}-E_{sl1}^{(b)}-E_{sl2}^{(b)})/2A, \tag{2}$$

where $E_{sl1}^{(b)}$ and $E_{sl2}^{(b)}$ are the bulk energies of the slabs, calculated for the slab size as given. To minimize numerical errors, the bulk energies are calculated with supercells similar to the ones used for interface calculations. The work of separation and the interface energy are not independent quantities, and one can be obtained from the other provided the surface energies are known. Here we present the results for both W_{sep} and γ. The purpose is to see which of these two descriptions is less sensitive to the choice of the model system, and can be more directly related to experiment.

The calculated values of the optimized interface interlayer separation, d_i, the work of separation, W_{sep}, and the interface energy, γ, for all the studied interface model systems are presented in Table IV. The important details of the atomic relaxations are given in Tables V and VI, with some notations in Fig. 4. The discussion below first considers the energetics of the unrelaxed interface structures, from the simplest 1Co/1Ti(C,N) interfaces to the more complex 5Co/4Ti(C,N) and 8Co/5Ti(C,N) interfaces. Then relaxation effects are analyzed, and comments are made on the obtained difference in the behavior between the ideal work of separation and the interface energy.

TABLE IV. Interface energetics. For each considered interface geometry (Fig. 2) the equilibrium distance between the Co and Ti(C,N) layers, d_i (see Fig. 3); the ideal work of separation [Eq. (1)] W_{sep}; and the interface energy [Eq. (2)] γ are displayed. Both unrelaxed (Unrel) and relaxed (Rel) values of W_{sep} and γ are given. In parentheses we show values obtained with the (5+5)-layer supercells.

Interface	d_i(Å)	W_{sep} (J/m^2)		γ (J/m^2)	
		Unrel	Rel	Unrel	Rel
1Co/1TiC-I	1.85	4.42 (4.47)	4.18 (4.27)	0.21 (0.18)	0.20 (0.16)
1Co/1TiC-II	2.4	0.68 (0.47)	0.46 (0.37)	3.95 (4.17)	3.91 (4.05)
5Co/4TiC-I	2.06	2.74	3.28	1.69	0.96
5Co/4TiC-II	2.08	2.60	3.25	1.83	0.98
8Co/5TiC-I	2.10	2.66	3.25 (3.45)	2.11	1.40 (1.25)
8Co/5TiC-II	2.10	2.67	3.22	2.11	1.43
1Co/1TiN-I	1.86	4.06 (4.11)	3.75 (3.76)	0.35 (0.38)	0.22 (0.32)
1Co/1TiN-II	2.5	1.28 (1.27)	0.95 (0.86)	3.13 (3.34)	3.02 (3.22)
5Co/4TiN-I	2.07	2.35	2.20	1.95	1.70
5Co/4TiN-II	2.03	2.31	2.70	1.99	1.20
8Co/5TiN-I	2.23	2.13	2.33 (2.42)	2.36	1.83 (1.76)
8Co/5TiN-II	2.23	2.11	2.11	2.38	2.05

The 1Co/1Ti(C,N) interfaces represent the most illustrative cases. For 1Co/1Ti(C,N)-I, when the interface Co atom is placed over the C or N atom (see Fig. 2), the equilibrium interface interlayer separation is noticeably less, by 0.15-0.3 Å, than the interlayer separation in bulk TiC and TiN or CoC and CoN. The work of separation for 1Co/1TiC-I and 1Co/1TiN-I is about 30% larger than the doubled values of the TiC(001) and TiN(001) surface energies (Table II). Thus the 1Co/1TiC-I or 1Co/1TiN-I interface bonding is stronger than the bonding between the TiC or TiN (001) bulk layers. Quite different features are observed when the Co atom is over the Ti atom [1Co/1Ti(C,N)-II interface]. In this case the equilibrium interface separation is as large as 2.4-2.5 Å, and W_{sep} becomes at least three times smaller than for 1Co/1Ti(C,N)-I.

Each of the more complex interface structures, 5Co/4Ti(C,N) and 8Co/5Ti(C,N), can be viewed as a mixture of different local configurations: some of the interface Co

TABLE V. Relaxations of the relative atomic positions. For a given pair of atoms, 1 and 2, the distance between them, r_{12}, before and after relaxation is presented. Only the pairs with unrelaxed or relaxed r_{12} distances less than 2.5 Å are included. The atom labels are as in Fig. 4. In parentheses there are numbers from the tests with the (5+5)-layer supercells.

Interface	Atoms		r_{12} (Å)			
			Co/TiC		Co/TiN	
	1	2	Unrel	Rel	Unrel	Rel
5Co/4Ti(C,N)-I	Ti	Co$^{[A]}$	2.28	2.36	2.28	2.37
	C(N)$^{[A]}$	Co$^{[A]}$	2.83	1.99	-	-
	C(N)$^{[B]}$	Co$^{[A]}$	2.47	2.10	2.47	2.46
	C(N)$^{[C]}$	Co$^{[B]}$	2.06	1.95	2.07	1.91
5Co/4Ti(C,N)-II	Ti$^{[B]}$	Co$^{[A]}$	2.49	2.68	2.43	2.60
	Ti$^{[C]}$	Co$^{[B]}$	2.08	2.36	2.03	2.28
	C(N)	Co$^{[A]}$	2.29	1.87	2.24	1.89
8Co/5Ti(C,N)-I	Ti$^{[B]}$	Co$^{[C]}$	2.24	2.38 (2.38)	2.35	2.37 (2.38)
	C(N)$^{[A]}$	Co$^{[A]}$	2.24	1.98 (1.98)	2.35	1.96 (1.95)
	C(N)$^{[B]}$	Co$^{[B]}$	2.71	2.03 (2.03)	-	-
8Co/5Ti(C,N)-II	Ti$^{[A]}$	Co$^{[A]}$	2.10	2.33	2.23	2.37
	Ti$^{[B]}$	Co$^{[B]}$	2.36	2.46	2.47	2.39
	C(N)$^{[A]}$	Co$^{[B]}$	2.36	2.04	2.47	2.14
	C(N)$^{[A]}$	Co$^{[C]}$	2.60	2.20	-	-
	C(N)$^{[B]}$	Co$^{[D]}$	2.10	1.93	2.23	1.93

TABLE VI. Perpendicular relaxation of the Ti(C,N) interface layer expressed in percent of the bulk Ti(C,N) interlayer spacing. For comparison, the free Ti(C,N)(001) surface relaxations are also included. The notations are the same as in Table V. The values in parentheses are for the 5+5 supercells.

Interface	Atom	Relaxation (%)	
		Co/TiC	Co/TiN
1Co/1Ti(C,N)-I	Ti	−1.6(−2.2)	4.8 (2.15)
	C(N)	−0.7(−0.6)	−2.1(−2.7)
1Co/1Ti(C,N)-II	Ti	−2.0(−3.9)	6.2(5.0)
	C(N)	1.0 (1.8)	−2.2(−3.2)
5Co/4Ti(C,N)-I	Ti	−2.4	1.2
	$C(N)^{[A]/[B]/[C]}$	61.3/11.6/1.6	−5.4/3.1/−0.9
5Co/4Ti(C,N)-II	$Ti^{[A]/[B]/[C]}$	−5.1/−2.9/−3.3	−2.1/1.8/1.3
	C(N)	0.6	−3.0
8Co/5Ti(C,N)-I	$Ti^{[A]/[B]}$	−4.0/−2.6(−3.9/−2.6)	−1.8/2.7(−1.8/1.9)
	$C(N)^{[A]/[B]}$	4.1/45.7 (4.6/46.4)	−0.8/−4.6(−0.7/−5.7)
8Co/5Ti(C,N)-II	$Ti^{[A]/[B]}$	0.3/−3.8	3.7/0.5
	$C(N)^{[A]/[B]}$	12.6/0.5	1.7/−1.0
Free Ti(C,N)(001)	Ti	−3.2	−5.7
	C(N)	1.8	2.8

atoms are over C(N) or Ti sites, but the majority are in intermediate positions (see Fig. 2). There are quite similar chances for a Co atom being near Ti or near C(N). In the context of structure-energy correlations, it is interesting to note that the unrelaxed W_{sep} values for all four complex structures, 5Co/4Ti(C,N)-I,II and 5Co/4Ti(C,N)-I,II, are close to the average of the unrelaxed W_{sep} values for the 1Co/1Ti(C,N)-I and 1Co/1Ti(C,N)-II interfaces (see Table IV). That is, the bonding at those complex interfaces behaves like a superposition of Co-C(N) and Co-Ti bonds, and can thus be understood in terms of the results for the simple 1Co/1Ti(C,N) interfaces.

When the atomic positions are allowed to relax, the structure and energetics of the 1Co/1Ti(C,N) interfaces change only slightly (Tables IV and VI). To describe the atomic relaxations at the more complex interfaces, special labels for the interface atoms are introduced, as shown in Fig. 4. The fourfold symmetry of the interface unit cells (see Fig. 2) is taken into account, and the independent atoms are enumerated by $A, B, \ldots$ from the unit-cell center to the corners. For the complex interfaces the dominating relaxation effect is the change of the Co-C(N) and Co-Ti bond lengths at the interface. Table V displays the distances between the neighboring interface atoms, r_{12}, for unrelaxed and relaxed structures. Before relaxation those distances are quite irregular. On the one hand, if relaxation is allowed, then the Co-C(N) distances tend to be 1.9–2.0 Å, which is close to the Co-C(N) distance at the 1Co/1Ti(C,N)-I interface (d_i in Table IV). That trend is more pronounced for the Co/TiC interfaces than or the Co/TiN ones: the Co-C bond length can decrease by up to 0.8 Å (see Table V). On the other hand, the distances between Co and Ti, unrelaxed being less than 2.4 Å, tend to increase to 2.4 Å after relaxation, i.e., close to the Co-Ti distance at the 1Co/1Ti(C,N)-II interfaces. Therefore, there is a similarity between the Co-C(N) or Co-Ti bonds at the complex interfaces and the corresponding bonds at the simplest 1Co/1Ti(C,N) interfaces.

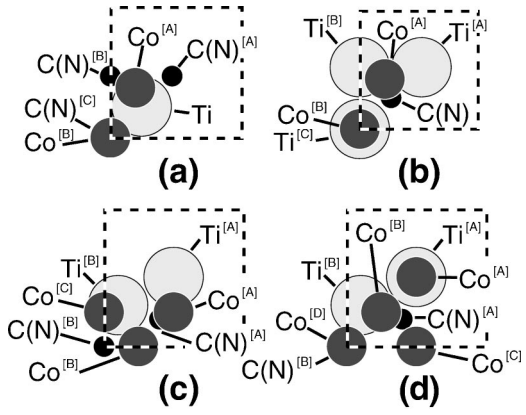

FIG. 4. Irreducible sets of atoms describing 5Co/4Ti(C,N) and 8Co/5Ti(C,N) interface geometries. (a) 5Co/4Ti(C,N)-I. (b) 5Co/4Ti(C,N)-II. (c) 8Co/5Ti(C,N)-I. (d) 8Co/5Ti(C,N)-II. The positions of the rest of atoms in (c)–(f) are determined by the fourfold rotational symmetry.

Interesting features are also observed in the perpendicular relaxation of the interface Ti(C,N) layer (Table VI). The Ti atoms of the TiC interface layer have the same (inward) direction and the same order of magnitude of perpendicular relaxation as for the free (001)TiC surface. Some Ti atoms are pushed a little more inward by the repulsion from Co. A very interesting effect is that if a C atom appears to be under an interstitial of Co, like $C^{[A]}$ at 5Co/4TiC-I or $C^{[B]}$ at 8Co/5TiC-I (see Figs. 2 and 4), it then relaxes very deep into

Co, by up to 45–60 % of the TiC interlayer distance, until the Co-C bond-length reaches 2.0 Å. That is to say that the interface Co-C bonds are strong enough to counteract the very strong Ti-C bonds. The behavior of the TiN interface layer differs from that of both Co/TiC and the free TiN(001) surface. The majority of Ti atoms goes a little outward, while the majority of the N atoms go inward (see Table VI). Such a type of relaxation is observed even for the simplest 1Co/1TiN interfaces. The obtained qualitative difference between the C(N) relaxations at Co/TiC and Co/TiN indicates that the TiC surface is much less stable in the presence of cobalt than the TiN surface. This can be connected to the experimental observation that the solubility of TiC in liquid Co is much higher than the solubility of TiN.[65]

The strengthening of the Co-C(N) bonds and the weakening of the Co-Ti repulsion upon the relaxation are reflected in the values of W_{sep} (see Table IV). As is the case for the changes in the atomic structure, the change in W_{sep} is larger for Co/TiC than for Co/TiN. In some cases, e.g., 5Co/4TiN-I, the relaxed value of W_{sep} is smaller than the unrelaxed one. This means that the relaxation changes the energies of the free slabs [E_{sl1} and E_{sl2} in Eq. (1)] more than the total energy of the interface system.

For all considered complex Co/TiC interfaces, the relaxed values of W_{sep} are practically the same, $W_{sep}=3.25 \pm 0.03$ J/m^2 (3+3 supercell), and they are only about 10% smaller than the value of W_{sep} measured in wetting experiments,[36] $W_{sep}=3.64$ J/m^2 (at 1500 °C). With 5+5 supercells, the result for the 8Co/5TiC-I interface, $W_{sep}=3.45$ J/m^2, is even closer to that experimental value. This is an experimental support for the realism of our model systems, i.e., that they incorporate the characteristic features of bonding at realistic Co/TiC interfaces.

In contrast to the case of Co/TiC, the relaxed W_{sep} values for Co/TiN interfaces vary quite significantly from one interface structure to another. This can be ascribed to the relative stability of the TiN interface layer. During the relaxation the interface N atoms do not move toward the Co interface layer to the same large extent as the C atoms at Co/TiC (see Table VI). This makes the relaxed W_{sep} values more sensitive to the initial (unrelaxed) interface structure.

Our results for the interface energy γ (see Table IV) are more sensitive to the choice of the model system, in particular to the Co phase. This sensitivity is enhanced by the fact that the absolute values of γ are noticeably smaller than the values of W_{sep}. That is, the same absolute changes cause substantially larger relative changes of γ than of W_{sep}. This can be seen most clearly by comparing the 5Co/4TiC and 8Co/5TiC interfaces. The relaxed work of separation is practically the same, but the interface energy changes by 0.4 J/m^2, i.e., by 40%.

The work of separation and the interface energy are related by $W_{sep}=\sigma_1+\sigma_2-\gamma$, where σ_1 and σ_2 are the surface energies of the slabs. According to Tables III and IV the difference between the 5Co/4TiC and 8Co/5TiC interface energies is equal to the difference between the surface energies of the corresponding Co phases. This indicates that the energy of the Co/TiC interface system contains contributions that are basically the same as for the free Co slabs. Such contributions are mostly sensitive to the Co phase. They are excluded from the work of adhesion, but contained in the interface energy γ.

In this context, there is one more important observation: In the above-mentioned wetting experiments,[36] the surface energy of liquid Co (at 1500°C), 1.88 J/m^2, is 1.1 J/m^2 smaller than our calculated values for PM fcc Co(001) at zero temperature (Table III). However, our result for W_{sep} of Co/TiC is only within 0.4 J/m^2 different from the measured high-temperature value.[36] These arguments allow us to conclude that in our study the work of separation is a more well-defined quantity than the interface energy. Reliable calculations of the interface energy require a more detailed and accurate description of the contacting phases and the interface structure.

B. Electronic structure

The results discussed above show that the Co/Ti(C,N) adhesion is mainly due to the strong chemical bonds between the Co and C or N atoms. Here we explore the nature of those bonds in terms of the electronic structure. As a starting point for our analysis we take the picture of metal-carbon and metal-nitrogen bonding in bulk transition-metal carbides and nitrides developed in Refs. 34 and 35: bulk bonding dominated by the strong covalent σ bonding between the d orbitals of the metal atoms and the $2p$ orbitals of C and N. The pd hybridization is most clearly seen in the electronic density of states (DOS). One can distinguish an energy region of bonding states separated by a DOS minimum from the regions of nonbonding and antibonding states. Filling of these bonding and antibonding states determines the trends in the cohesive energy of the carbides and nitrides. It is controlled by the average number of electrons per atom (n_e), with the strongest bonding at $n_e=4$. Among the $3d$ transition-metal carbides and nitrides, TiC ($n_e=4$) has the largest cohesive energy because the Fermi level is at the minimum (pseudogap) between the energy intervals of the bonding and antibonding states. For TiN, $n_e=4.5$, and the cohesive energy is smaller (see Table I). There is even weaker bonding for CoC and CoN, due to substantial filling of the antibonding states (n_e is 6.5 and 7.0, respectively). In this context, the main questions are whether the Co-C(N) bonds at the Co/Ti(C,N) interfaces are governed by the same rules as in bulk carbonitrides, and, if so, why the interface Co-C(N) bonds can be stronger than even the Ti-C(N) bonds in bulk Ti(C,N).

Below we present only the results for the unrelaxed 1Co/1Ti(C,N)-I and relaxed 8Co/5Ti(C,N)-I interfaces obtained with (5+5)-layer supercells. As can be seen from Sec. IV A, these interface structures incorporate practically all important features of the other considered model system.

A very pronounced behavior is observed for the electron density distribution [Figs. 5 and 6]. Figure 5 displays the electron density for the 1Co/1Ti(C,N)-I interfaces [Figs. 5(a) and 5(b)] compared to the Co(C,N) bulk [Figs. 5(c) and 5(d)]. In this figure one can distinguish a localized chemical bond between the interface Co and C(N) atoms with a high electron density along the Co-C(N) line. The electron density

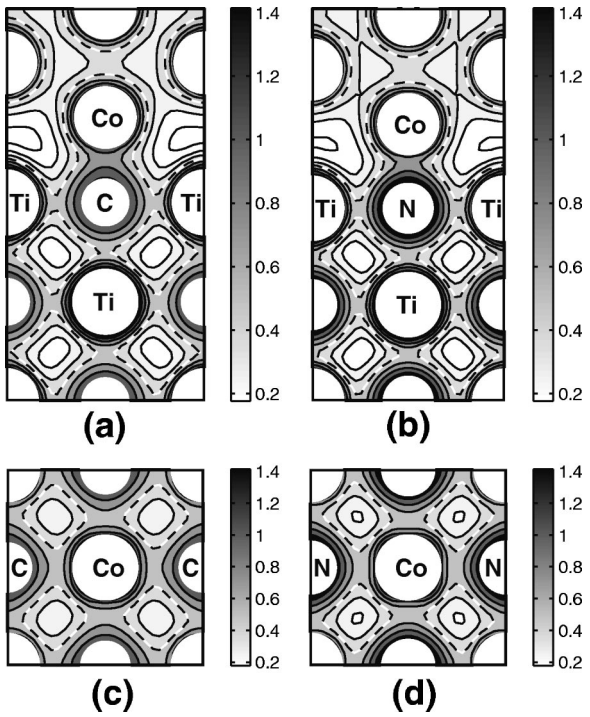

FIG. 5. Valence electron density for the ideal (unrelaxed) 1Co/1TiC-I (a) and 1Co/1TiN-I (b) interfaces [(5+5)-layer supercells], compared to bulk CoC (c) and CoN (d). The (010) cuts are shown. The consecutive contours change by a factor of $\sqrt{2}$. The color bars are in units of electrons/Å^3. The dashed line is at the level of 0.5 electrons/Å^3. Only the density distribution outside the atomic cores is presented.

at the interface Co-C(N) bond is about 1.4 times higher than at the Co-C(N) bonds in bulk Co(C,N) or at the Ti-C(N) bonds in the bulk layers of Ti(C,N). An analogous situation exists with Co-C(N) bonds at 8Co/5Ti(C,N)-I interfaces (Fig. 6). Figure 6 also gives more evidence of the dominance of interface Co-C(N) bonding over Co-Ti bonding. It can be noted that the energetics of the interface Co-C(N) bonds discussed above is quite strongly correlated with the magnitude of the electron density at those bonds. Thus the spatial distribution of the electron density indicates that the interface Co-C(N) bonds have a predominantly covalent character.

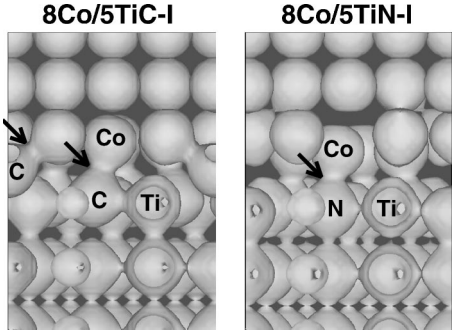

FIG. 6. Valence electron density for the relaxed 8Co/5TiC-I and 8Co/5TiN-I interfaces [(5+5)-layer supercells]. The constant-density surfaces at the level of 0.5 electrons/Å^3 are presented. The arrows point at the interface Co-C(N) bonds.

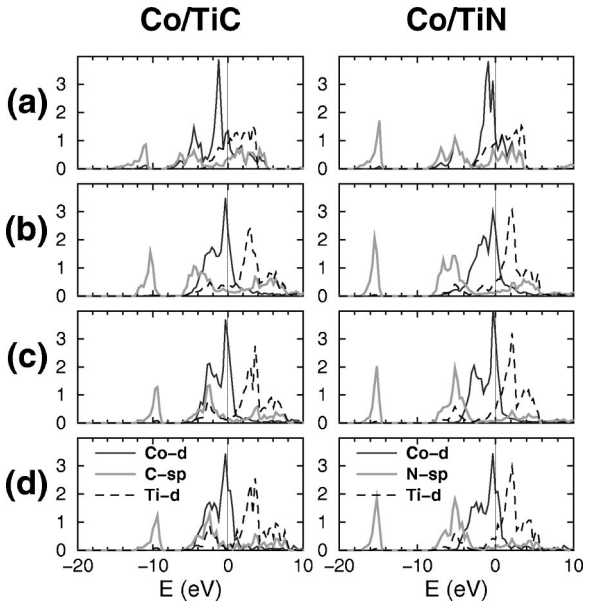

FIG. 7. 1Co/1TiC-I and 1Co/1TiN-I interfaces (unrelaxed, 5+5 supercells): Local density of states projected onto the atomic orbitals (number of states per eV per atomic sphere): (a) for Co and C(N) atoms in bulk Co(C,N), and for a Ti atom in bulk fcc Ti; (b) for atoms in the interface layers of 1Co/1Ti(C,N)-I; (c) for atoms one layer off from the interfaces; and (d) in the corresponding bulk phases of Co and Ti(C,N).

A more detailed picture of how Co/Ti(C,N) interface bonds are formed can be extracted from the analysis of the electronic local DOS (LDOS) projected onto different atomic orbitals (Figs. 7 and 8). In Fig. 7 we present the main components of the projected LDOS for the 1Co/1Ti(C,N)-I interface systems [Figs. 7(b) and 7(c)] in comparison with the corresponding bulk materials [Figs. 7(a) and 7(d)]. In the projected LDOS of the bulk CoC and CoN [Fig. 7(a)], the boundaries between bonding and antibonding states (pseudogaps) are between about -4 and -3 eV. The bonding states are seen as resonance peaks in the Co-*d* and C(N)-*p* LDOS's between -8 and -4 eV. The antibonding states are derived mainly from the *d* orbitals of Co, and they are almost filled. There is a similar picture for bulk TiC and TiN [Fig. 7(d)], but the Fermi level is near the pseudogap.

Compared to bulk Co and Ti(C,N) the 1Co/1Ti(C,N)-I interface systems have some interesting features in the projected LDOS of the interface layers [Fig. 7(b)]. The C(N)-*sp* LDOS is closer to the C(N)-*sp* LDOS of bulk Co(C,N). This can be ascribed to the formation of the interface Co-C(N) bonding states. The Co-C(N) bonding partially destroys the Ti-C(N) bonding states. In the Ti-*d* LDOS the resonance peaks from the Ti-C(N) bonding states are broadened and are of smaller height. In addition, there are more Ti-*d* states in the pseudogaps. As seen from Fig. 7(c), the subsurface LDOS of the Co and Ti(C,N) looks almost like that of the corresponding bulk materials [Fig. 7(d)].

Figure 8 displays the projected LDOS of different layers of the relaxed 8Co/5Ti(C,N)-I interfaces. It is organized in the same way as Fig. 7, to clearly show that the main features are basically the same as those for the 1Co/1Ti(C,N)-I.

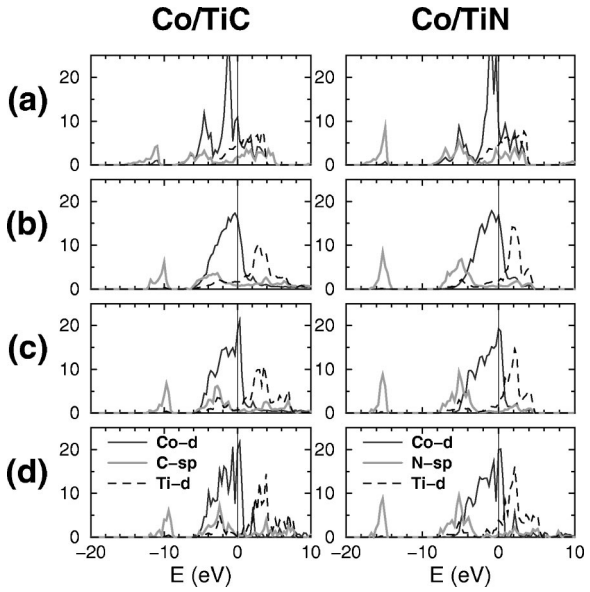

FIG. 8. Local density of states (LDOS) of different layers of the relaxed 8Co/5Ti(C,N)-I interfaces (5+5 supercells) compared to the corresponding bulk materials. Here the local density of a given layer is calculated as a sum of the projected LDOS's of all identical atoms of that layer within one interface supercell [eight, five, and five atoms of Co, C(N) and Ti, respectively]. (a) Projected LDOS for eight atoms of Co and five atoms of C(N) in bulk Co(C,N), and for five Ti atoms in bulk fcc Ti. (b) LDOS of the interface layers of 8Co/5Ti(C,N)-I. (c) LDOS of the Co and Ti(C,N) layers one layer off from the interfaces. (d) LDOS of the corresponding layers in bulk Co and Ti(C,N).

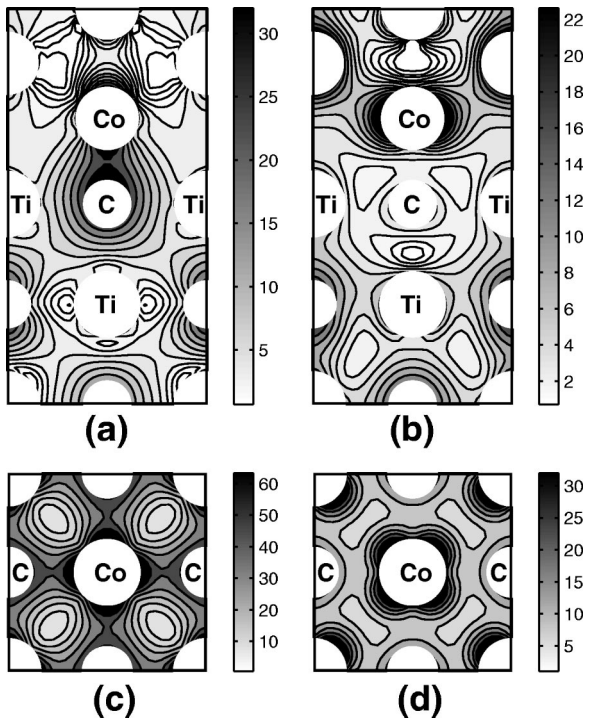

FIG. 9. Real-space behavior of the 1Co/1TiC-I interface bonding (a) and antibonding (b) states compared to bulk CoC bonding (c) and antibonding (d) states. The (010)-cut contour plots of the electron-density contributions from different Kohn-Sham bands are presented. The consecutive contours change by a factor of $\sqrt{2}$, and the color bars are in units of millielectrons/Å^3. Plots (a)–(d) correspond to bands in energy intervals of -4.7––3.7, -2.5––1.7, -4.9––2.6, and -2.5––1.3 eV, respectively.

Another interesting observation concerns the interface LDOS in Figs. 7(b) and 8(b). The formation of the Co-C(N) bond should normally also give antibonding states. However, there are no pronounced resonances from interface Co-C(N) antibonding states. The Co-*d* component is much closer to the Co-*d* LDOS in bulk Co [Figs. 7(d) and 8(d)] than in bulk Co(C,N) [Figs. 7(a) and 8(a)]. The explanation suggested here is that the Co-C(N) antibonding states are broadened in space and energy due to their coupling to the delocalized metallic states of cobalt. To clarify this statement, let us consider how the bulk Co-C(N) bonds should be modified when they are transferred into the Co/Ti(C,N) interface environment. In bulk Co(C,N), the major component of the Co-C(N) antibonding states is Co-*d*, i.e., states mainly localized around the Co atoms. At the interface, near the Co-C(N) bonds, there is a large concentration of metallic Co states with energies in the same region as we would expect for the Co-C(N) antibonding states. Then the Co-C(N) antibonding states are expected to hybridize significantly with the metallic states of the surrounding Co metal. This hybridization broadens the Co-C(N) antibonding states in space and energy, in the same way as the atomic levels of each atom of bulk Co are broadened into metallic states through the hybridization with the metallic states of the rest of the Co metal. Thus, at the interface, the Co-C(N) antibonding states are spread over larger regions of space and energy than in bulk Co(C,N). Hence they lose their antibonding action. Moreover, such a transformation of the Co-C(N) antibonding states should also affect the Co-C(N) bonding states, leaving more space for an accumulation of those bonding states along the Co-C(N) bonds. This is reflected in the charge density distribution in Figs. 5 and 6. This picture of metal-modified interface antibonding and bonding states also explains why the Co-C(N) bonds at the interface are stronger than even the Ti-C(N) bonds in bulk.

More insight into the real-space behavior of the interface bonding and antibonding states is given by an analysis of the contributions to the electron density from different Kohn-Sham bands, $n_i(\mathbf{r})$. Here $\mathbf{r}=\{x,y,z\}$ is a point in the real space. To calculate $n_i(\mathbf{r})$, the squared absolute values of the Kohn-Sham wave functions, $|\psi_{i\mathbf{k}}(\mathbf{r})|^2$, for some specific band i are integrated over the first Brillouin zone in $\mathbf{k}$ space. For simplicity, we restrict our analysis to the Co/TiC case. As one can see from the LDOS plots in Fig. 7, the most important Co-C bonding and antibonding states concentrate in the energy interval between -5.5 and 0 eV. Within that interval the different bands for which $n_i(\mathbf{r})$ has noticeable interface components are considered, and comparisons with the corresponding bulk CoC states are made.

Figure 9 shows representative examples of $n_i(\mathbf{r})$ for the unrelaxed 1Co/1TiC-I interface [Figs. 9(a) and 9(b)] and the bulk CoC [Figs. 9(c) and 9(d)]. The bands with $n_i(\mathbf{r})$, having

a strong bonding character, belong mainly to the energy region between -5.5 and -3.0 eV. The typical behavior of $n_i(\mathbf{r})$ for such states is displayed in Figs. 9(a) and 9(c). Those states are localized mainly along the Co-C bonds. There are quite explicit indications of the Co-C covalent σ bonding. At higher energies, at approximately -3.0 or -2.5 eV there are states with more and more metallic Co character, and the bonding components are less and less pronounced. For some bands there are features of Co-C π bonding.

The characteristic features of Co-C antibonding are most clearly seen in the bulk CoC states [Fig. 9(d)]. The electronic density is localized quite strongly, being squeezed into the regions off from the Co-C bonds. At the Co/TiC interface, in the energy region between -2.5 and 0 eV, one can expect to find some signs of the Co-C antibonding states. A typical pattern of $n_i(\mathbf{r})$ for bands in that interval is shown in Fig. 9(b). The antibonding features are relatively hard to extract. The states of that energy region have predominantly metallic Co character, being quite delocalized in space and energy. In addition to what is shown in Fig. 9, closer to the Fermi level, between -1.5 and 0 eV one can also find indications of metallic bonding between Co and Ti. Finally, the picture given by the analysis of the electron-density contributions of separate Kohn-Sham bands is quite in line with our results for the valence electron density and the projected LDOS.

The above picture of the metal-modified strong covalent Co-C(N) bonds also allows one to understand the differences between the behavior of the Co/TiC and Co/TiN interfaces. In general, the hybridization of the electronic states that leads to formation of a covalent bond occurs mainly between the states that are close in energy. Let us note that at the Co/Ti(C,N) interfaces the energy positions of the C(N)-*p* and Ti-*d* states remain close to the positions they have in bulk Ti(C,N) (see Figs. 7 and 8). The main difference between TiC and TiN lies in the fact that TiN has one extra electron per Ti-N pair. This shifts the energy positions of the N-*p* and Ti-*d* states with respect to the Fermi level toward lower energies, i.e., more filling. As can be seen in Figs. 7 and 8, on the one hand, this shift moves the N-*p* states off from the Co-*d* states, reducing the covalency of the interface Co-N bonds. On the other hand, the Ti-*d* states become closer in energy to the Co-*d* states, which allows stronger Ti-Co bonding. Those two effects explain the stronger adhesion for Co over C (1Co/1TiC-I; Table IV) than for Co over N (1Co/1TiN-I), and also the stronger Co-Ti bonding at the 1Co/1TiN-II interface than at the 1Co/1TiC-II interface. The fact that the interface Co-N bonds are weaker than the Co-C bonds is clearly seen in the adhesion energies for the more complex structures (Table IV), as well as in the relaxation effects (Tables V and VI), as discussed in Sec. IV A.

V. CONCLUSIONS

In this paper an *ab initio* theoretical study of the atomistic nature of bonding at the Co/TiC and Co/TiN interfaces is presented. The energetics and electronic structure of the interfaces between the (001) face of fcc nonmagnetic cobalt and the (001) surfaces of TiC and TiN are investigated by means of self-consistent total-energy calculations in the framework of the density functional theory with the GGA-PW91 approximation for the exchange-correlation energy. For calibration of the plane-wave pseudopotential method used, various bulk properties of Co, Ti, Ti(C,N), and Co(C,N) are calculated, along with the surface properties of Co and Ti(C,N). In such tests a satisfactory agreement with the available experimental data and the results of other first-principles methods is demonstrated.

An approach to the analysis of the interface systems with large lattice mismatch is proposed. In this approach different high-symmetry model systems are compared in order to extract behaviors that are independent of a particular structural ordering. Such behaviors are expected to be present in more realistic complex-structured interface systems.

For all four complex Co/TiC interfaces considered, the relaxed values of the work of separation are within about 10% close to the value of the work of adhesion for liquid cobalt on the TiC surface measured in wetting experiments.[36] For Co/TiN interfaces, the relaxed values of the work of separation are more sensitive to the interface structure, and they are by about 0.6–1.0 J/m^2 lower than for Co/TiC.

It is found that the main mechanism of the interface adhesion between Co and TiC(001) or TiN(001) is provided by the strong Co-C(N) chemical bonds. The analysis of the energetics and the structure relaxation effects shows that the interface Co-C(N) bonds are noticeably stronger than the same bonds in bulk Co(C,N) or even the Ti-C(N) bonds in bulk Ti(C,N).

An interesting effect is found in the relaxation of the TiC surface at the Co/TiC interfaces. If an interstitial of the Co surface layer lies over the surface C atom, then the C atom goes very much inside the Co phase, by 45–60% of the TiC interlayer distance. This is very much in contrast with the situation at the Co/TiN interface. The perpendicular relaxation of the N atoms at Co/TiN is only a few percent, and many of these atoms even move inward the TiN slab. This drastic difference between the behaviors of C and N atoms at Co/TiC and Co/TiN, respectively, can be responsible for the known experimental fact that the solubility of TiC in liquid Co is much higher than the solubility of TiN.

Our analysis of the electronic structure of the Co/Ti(C,N) interface shows that the strong interface Co-C(N) bonds are covalent σ bonds between Co-3*d* and C(N)-2*p* orbitals. The relative strength of those bonds, indicated by our results for the atomic structure and energetics, is also reflected in the distribution of the valence electron density. The electron density along the Co-C(N) bonds at the interfaces is noticeably higher than at the Co-C(N) and Ti-C(N) bonds in bulk Co(C,N) and Ti(C,N), respectively. On the basis of the analysis of the electronic local density of states projected onto different atomic orbitals and of the electron-density contributions from different Kohn-Sham bands, we suggest that the observed strengthening of the Co-C(N) bonding at the interfaces is due to interface-induced modifications of the Co-C(N) bonding and antibonding states. Those modifica-

tions originate from the coupling between the Co-C(N) antibonding states and the metallic states of the Co phase, which leads to a delocalization of the Co-C(N) antibonding states in space and energy. In short, the interface Co-C(N) bonds can be described as metal-modified covalent bonds.

The difference in the adhesion strength and the relaxation effects between the Co/TiC and Co/TiN interfaces can be rationalized in terms of the relative positions of the energy regions of the Co-3*d* band and C-2*p* or N-2*p* bands. At Co/TiN, due to the extra electron of the N atom, the N-2*p* states are shifted more off in energy from the Co-3*d* states than the C-2*p* states at Co/TiC. This shift reduces the strength of covalent bonding between Co and N.

ACKNOWLEDGMENTS

The motivation for this work originateds from discussions with U. Rolander, Sandvik Coromant AB, and H.-O. Andrén, Chalmers. We are also thankful to J. Hartford, E. Schröder, Y. Yourdshayan, and L. Bengtsson for helpful discussions, and to C. Ruberto for critical comments on the manuscript. This work was partially supported by the Swedish Foundation for Strategic Research (SSF) via the Materials Consortia #9 and ATOMICS. Allocation of computer time at the UNICC facilities at Chalmers University of Technology and at the National Supercomputer Center at Linköping University is gratefully acknowledged.

*On leave from Institute for Radiophysics and Electronics, National Academy of Sciences Ukraine, Kharkov, Ukraine

[1] H.E. Exner, Int. Met. Rev. **24**, 149 (1979).
[2] J. Gurland, Int. Mater. Rev. **33**, 151 (1988).
[3] M.W. Finnis, J. Phys.: Condens. Matter **8**, 5811 (1996).
[4] F. Ernst, Mater. Sci. Eng., R. **14**, 97 (1995).
[5] K.H. Johnson and S.V. Pepper, J. Appl. Phys. **53**, 6634 (1982).
[6] K. Nath and A.B. Anderson, Phys. Rev. B **39**, 1013 (1989).
[7] M. Kohyama, S. Kose, M. Kinoshita, and R. Yamamoto, J. Phys. Chem. Solids **53**, 345 (1992).
[8] C. Noguera and G. Bordier, J. Phys. III **4**, 1851 (1994).
[9] P. Alemany, R.S. Boorse, J.M. Burlitch, and R. Hoffmann, J. Chem. Phys. **97**, 8464 (1993).
[10] P. Alemany, Surf. Sci. **314**, 114 (1994).
[11] A.M. Stoneham and P.W. Tasker, J. Phys. C **18**, L543 (1985).
[12] M.W. Finnis, Acta Metall. Mater. **40**, S25 (1992).
[13] D.M. Duffy, J.H. Harding, and A.M. Stoneham, Philos. Mag. A **67**, 865 (1993).
[14] U. Schönberger, O.K. Andersen, and M. Methfessel, Acta Metall. Mater. **40**, S1 (1992).
[15] Chun Li, Ruqian Wu, and A.J. Freeman, Phys. Rev. B **48**, 8317 (1993).
[16] J. Goniakowski, Phys. Rev. B **58**, 1189 (1998).
[17] R. Benedek, A. Alavi, D.N. Seidman, L.H. Yang, D.A. Muller, and C. Woodward, Phys. Rev. Lett. **84**, 3362 (2000).
[18] Yu.F. Zhukovskii, E.A. Kotomin, P.W.M. Jacobs, and A.M. Stoneham, Phys. Rev. Lett. **84**, 1256 (2000).
[19] I.G. Batirev, A. Alavi, M.W. Finnis, and T. Deutsch, Phys. Rev. Lett. **82**, 1510 (1999).
[20] C. Verdozzi, D.R. Jennison, P.A. Schultz, and M.P. Sears, Phys. Rev. Lett. **82**, 799 (1999).
[21] A. Bogicevic and D.R. Jennison, Phys. Rev. Lett. **82**, 4050 (1999).
[22] M. Hohyama and J. Hoekstra, Phys. Rev. B **61**, 2672 (2000).
[23] J. Hartford, Phys. Rev. B **61**, 2221 (2000).
[24] A.M. Stoneham, M.M.D. Ramos, and A.P. Sutton, Philos. Mag. A **67**, 797 (1993).
[25] L. Ramqvist, Jernkontorets Ann. **153**, 159 (1969).
[26] H. Goretzki, H.E. Exner, and W. Scheuermann, in *Modern Developments in Powder Metallurgy* edited by H.H. Hausner (Plenum, New York, 1971), Vol. 4, p. 327.
[27] H. Goretzki and W. Scheuermann, in *Preprints of 7th Plansee Seminar* (Planseewerke, Reutte, 1971), Vol. 4, Paper No. 50.
[28] R.G. Barrera and C.B. Duke, Phys. Rev. **13**, 4477 (1976).
[29] P. Xiao and B. Derby, Acta Metall. Mater. **44**, 307 (1996).
[30] S.V. Dudiy, J. Hartford, and B.I. Lundqvist, Phys. Rev. Lett. **85**, 1898 (2000).
[31] P. Hohenberg and W. Kohn, Phys. Rev. B **136**, B864 (1964).
[32] W. Kohn and L. Sham, Phys. Rev. A **140**, A1133 (1965).
[33] R.O. Jones and O. Gunnarsson, Rev. Mod. Phys. **61**, 689 (1989).
[34] J. Häglund, G. Grimvall, T. Jarlborg, and A.F. Guillermet, Phys. Rev. B **43**, 14 400 (1991).
[35] J. Häglund, A.F. Guillermet, G. Grimvall, and M. Körling, Phys. Rev. B **48**, 11 685 (1993).
[36] L. Ramqvist, Int. J. Powder Metall. **1**, 2 (1965).
[37] M. Rettenmayr, H.E. Exner, and W. Mader, Mater. Sci. Technol. **4**, 984 (1988).
[38] G.E. Hollox, Mater. Sci. Rep. **3**, 121 (1968).
[39] S.A. Horton, M.B. Waldron, B. Roebuck, and E.A. Almond, Powder Metall. **27**, 201 (1984).
[40] S. V. Dudiy (unpublished).
[41] M. Aldén, H.L. Skriver, S. Mirbt, and B. Johansson, Surf. Sci. **315**, 157 (1994).
[42] J.P. Perdew, J.A. Chevary, S.H. Vosko, K.A. Jackson, M.A. Pederson, D.J. Singh, and C. Fiolhais, Phys. Rev. B **46**, 6671 (1992).
[43] V. Ozoliņš and M. Körling, Phys. Rev. B **48**, 18 304 (1993).
[44] R. Ahuja, O. Eriksson, J.M. Wills, and B. Johansson, Phys. Rev. B **53**, 3072 (1996).
[45] M.C. Payne, M.P. Teter, D.C. Allan, T.A. Arias, and J.D. Joannopoulos, Rev. Mod. Phys. **64**, 1045 (1992).
[46] G. Kresse and J. Furthmüller, Phys. Rev. B **54**, 11 169 (1996).
[47] G. Kresse and J. Hafner, J. Phys.: Condens. Matter **6**, 8245 (1994).
[48] L. Hansen *et al.*, Dacapo-1.30, Center for Atomic Scale Materials Physics (CAMP), Denmark Technical University.
[49] D. Vanderbilt, Phys. Rev. B **41**, 7892 (1990).
[50] S.G. Louie, S. Froyen, and M.L. Cohen, Phys. Rev. B **26**, 1738 (1982).
[51] H.J. Monkhorst and J.D. Pack, Phys. Rev. B **13**, 5188 (1976).
[52] M.J. Gillan, J. Phys.: Condens. Matter **1**, 689 (1989).
[53] C. Kittel, *Introduction to Solid State Physics*, 7th ed. (Wiley, New York, 1996).
[54] R.W.G. Wyckoff, *Crystal Structures*, 2th ed. (Interscience, New York, 1963), Vol. 1.
[55] F.D. Murnaghan, Proc. Natl. Acad. Sci. U.S.A. **30**, 244 (1944).
[56] A.T. Paxton, M. Methfessel, and H.M. Polatoglou, Phys. Rev. B **41**, 8127 (1990).

[57] Y. Yourdshahyan (unpublished).
[58] E.G. Moroni, G. Kresse, J. Hafner, and J. Fürthmüller, Phys. Rev. B **56**, 15 629 (1997).
[59] M. Körling and J. Häglund, Phys. Rev. B **45**, 13 293 (1992).
[60] V. Fiorentini and M. Methfessel, J. Phys.: Condens. Matter **8**, 6525 (1996).
[61] D.L. Price, J.M. Wills, and B.R. Cooper, Phys. Rev. Lett. **77**, 3375 (1996).
[62] Y. Kido, T. Nishimira, Y. Hoshino, S. Otani, and R. Souda, Phys. Rev. B **61**, 1748 (2000).
[63] M. Aono, Y. Hou, R. Souda, C. Oshima, S. Otani, and Y. Ishizawa, Phys. Rev. Lett. **50**, 1293 (1983).
[64] A.Y. Liu and D.J. Singh, Phys. Rev. B **47**, 8515 (1993).
[65] P. Ettmayer, H. Kolaska, W. Lengauer, and K. Dreyer, Int. J. refract. Met. Hard Mater. **13**, 343 (1995).